Parameters of light-induced charge transfer processes in photorefractive crystals

© O.F. Schirmer, C. Veber, M. Meyer

Fachbereich Physik, Universität Osnabrück,
D-49069 Osnabrück, Germany

A method is outlined by which the parameters governing light-induced charge transfer processes in photorefractive crystals can be determined. The system $BaTiO_3:Rh$ is treated as an example. EPR is used to obtain information on the EPR-active defect charge states. By simultaneous observation of light-induced EPR- and optical absorption changes the corresponding optical absorption bands are established as fingerprints of the defect charge states. Consistency arguments allow to label also EPR-silent absorption bands in this way, significantly extending the scope of EPR based defect studies. On this basis the charge transfer paths taking place under illumination are identified. Quantitatively, the defect concentrations are directly on indirectly derived from the available EPR signals. In addition the kinetics of the light-induced changes of the densities of the occurring defect charge states are studied. In conjunction with the defect concentrations, this allows to deduce the responsible transfer parameters.

The photorefractive effect in a suitable electro-optic material is usually triggered by the photoionisation of defects [1]. Under illumination with an inhomogeneous light pattern the freed charge carriers are moving in either the valence or in the conduction band from the brighter regions towards the darker ones, transported by various possible driving mechanisms. A charge pattern results; it is accompanied by the corresponding space charge field, which is transformed into a refractive index pattern by the electro-optic effect. Fig. 1 demonstrates the three elementary models under which the occurring charge transfer processes can be subsumed [2]. In the 1-center model, the defects representing source and drain of the charge carriers are indentical. In the two other models, 2-centre and 3-valence model, the carriers end at levels different from the initial ones. In the latter situations, photochromism is usually observed, since each of the defect charges absorbs light in different ways. It should be noted that such absorption changes occur also under homogeneous illumination. For a quantitative prediction to the photorefractive performance of a material it is necessary to know the concentrations of the defects in the various possible charge states and their spatial distributions present under defined illumination conditions. These quantities can be obtained, if a set of parameters is known describing the kinetics of the light-induced charge transfers between the relevant defects. In a later section these parameters will be introduced.

The essential role of defects in the photorefractive effect is obvious. Because of this reason the structure and properties of defects in several inorganic photorefractive crystals have been investigated intensively during the last decade, mainly by EPR studies ($BaTiO_3$, $LiNbO_3$, $Sr_{1-x}Ba_xNbO_6$, $KNbO_3$, $Ba_{1-x}Ca_xTiO_3$, $Bi_{12}MO_{20}$ ($M = Ti, Ge, Si$), etc.) [3–5]. At this point it is advantageous to demonstrate a way how the charge transfer processes connected with the defects can be elucidated from the information available about them. If a method can be outlined how this knowledge leads to insight into the charge transfer processes connected with the defects, an important step towards an understanding of the optical properties of the materials has been achieved.

The term 'defect' can be used with two different meanings; first it may stand for a certain chemical entity which interrupts the periodicity of a crystal lattice, and second, for one of the charge states such a perturbation can acquire. In the latter case we shall talk of 'defect charge state', if necessary.

The procedure which we developed to quantitatively assess the role of defects in charge transfer processes, especially in photorefractive crystals, will be exemplified in the

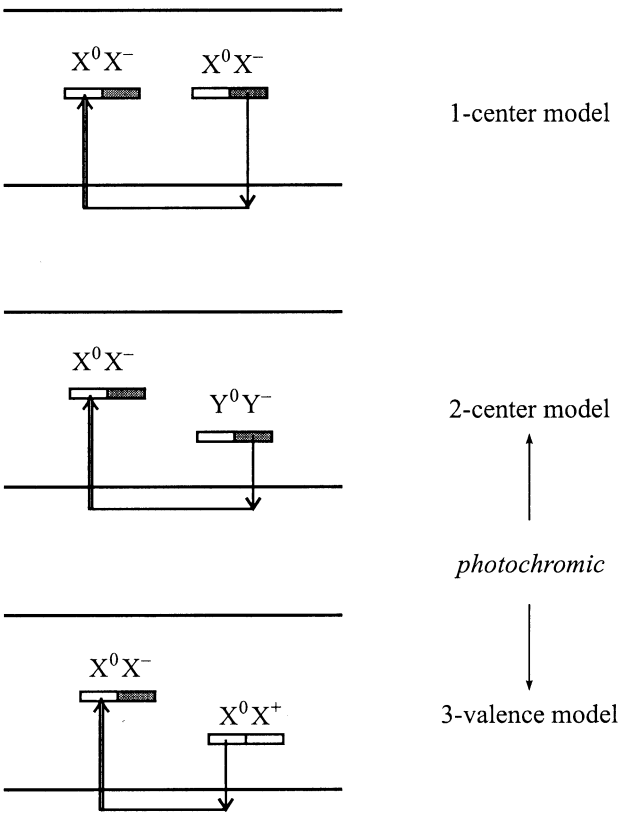

Figure 1. The three basic models for charge transfer processes between defect gap levels. The lower two lead to light-induced optical absorption under homogeneous illumination.

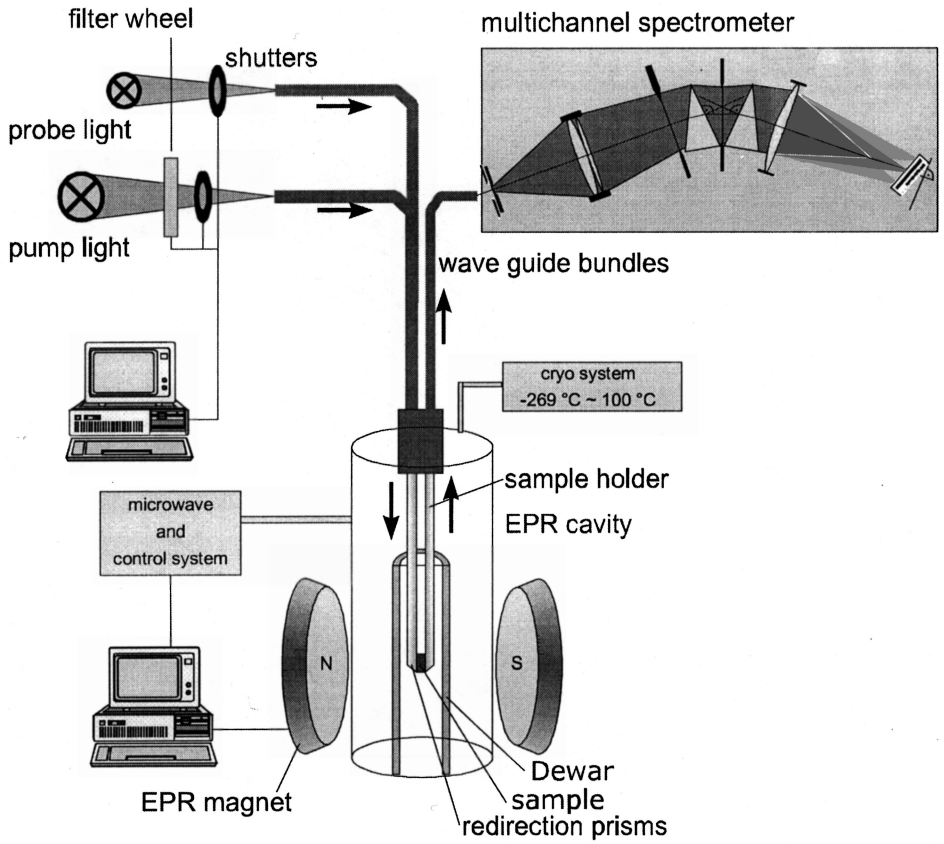

Figure 2. Setup for combined EPR/optical absorption investigations of light-induced signal changes. The specimen, centred in the EPR cavity between two half-cylindrical quartz rods, is first illuminated by intense monochromatic pump light for typically 60 s; the resulting signal changes are then simultaneously probed by EPR and weak, 1–3 eV, 20 ms pulsed white probe light. The transmitted light, guided by prisms at the quartz rods, is dispersed and registered with a multichannel detector.

following by the system $BaTiO_3$ doped with Rh. This host lattice has high electrooptic coefficients; therefore only a few transferred charges can already head to measurable index changes, and thus the material offers high photorefractive sensitivity. Doping with Rh increases the infrared response of the system [6–10].

1. Method

If applicable, EPR is the most suitable method to obtain information on the chemical, geometrical, electronic and energetic structure of defects. However, in many cases defects are EPR-silent. Since these can likewise be involved in the charge transfer processes, one has to look for ways to get information on them also. The method which we introduced is able to achieve this and will eventually allow to get the quantitative information needed to predict the defect-induced photorefratice properties. In this section the procedure is outlined briefly. The first step is to establish the optical absorption bands as fingerprints of the defects on the basis of the available EPR information. As will be shown, this can be done not only for EPR-active, but also for EPR-silent defects. By comparing the defect concentrations, deduced from the EPR intensities, to the absorption strengths, also the optical cross-sections of the absorption bands are obtained. From here on, all further studies can be based on optical measurements alone. Usually these can be performed at room temperature, where EPR investigations generally fail, but where photorefractive devices are expected to operate. The changes of the optical absorption bands under illumination with pump light allows to draw conclusions about the charge transfer processes taking place at these pump energies. Also the defect concentrations present under the various experimental illumination conditions can be deduced. Further parameters describing the charge transfer processes are deduced from the temporal evolution of the defect concentrations occurring after switching the lihgt on or off.

2. Qualitative identification of the charge transfer processes

The experimental data mentioned in the following is taken from the investigation of a $BaTiO_3:Rh$ crystal grown from a $BaTiO_3$ melt unintentionally containing rhodium. The simultaneous observation of light-induced EPR- and optical

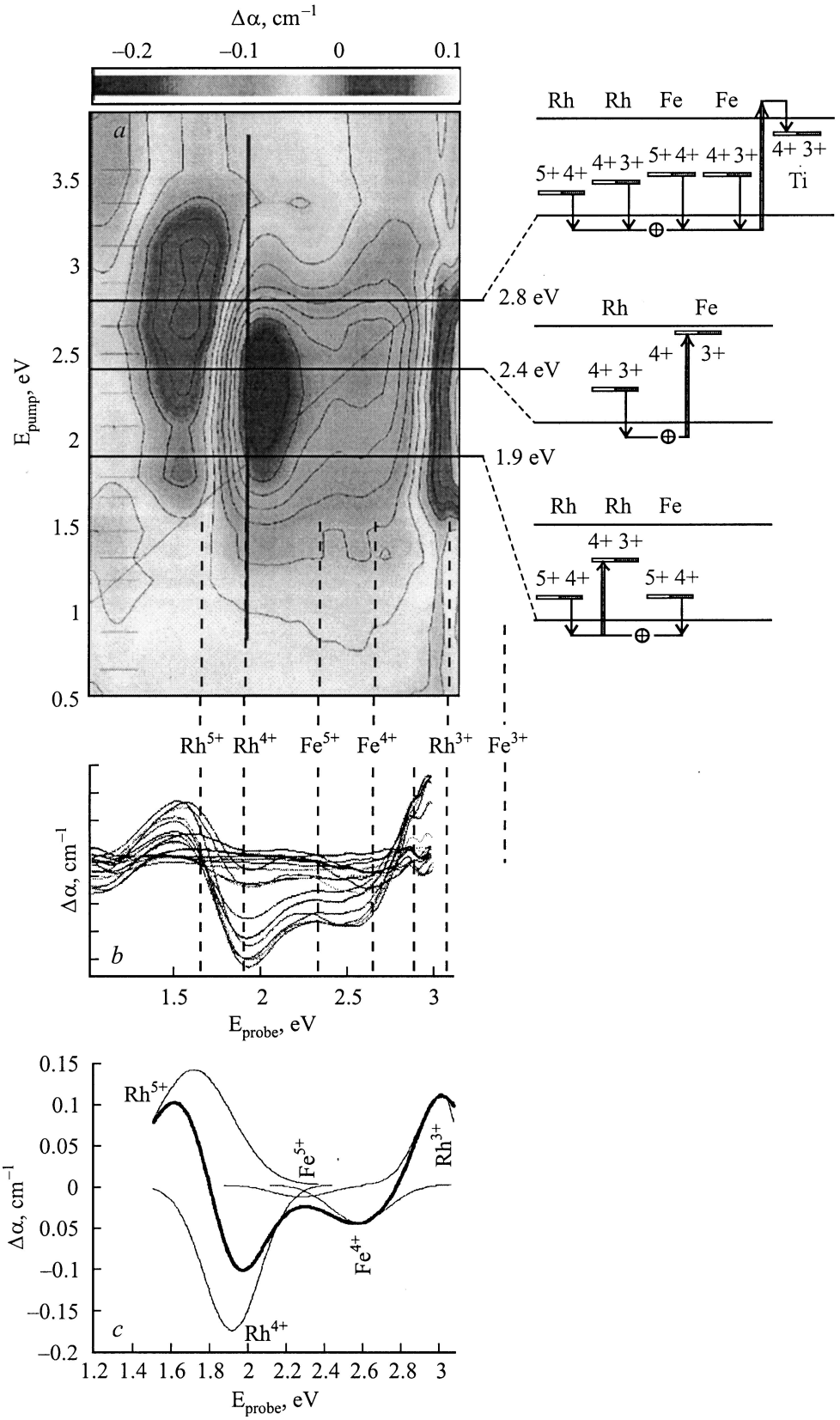

Figure 3. *b* — optical absorption changes of $BaTiO_3$: Rh after illumination with 17 different pump energies. *a* — same information plotted in a pseudo-3*D* plot. Abscissa: probe light energy. Ordinate: pump light energy. Grey shading: absorption changes, as calibrated by bar on top. Assignment to the various charge states of Rh and Fe is indicated by the dashed lines. The thick vertical line is addressed in Fig. 4. An analysis of the plot into its component bands is shown in panel *c* (state after 1.9 eV pumping). The variation of the plot under different pumping energies is analysed at the right by the appropriate level schemes.

absorption changes is performed with a setup described earlier [11] allowing optical absorption measurements within an EPR cavity in a rather flexible way. A scheme is presented in Fig. 2. Absorption changes, resulting when the pump light energy is increased stepwise, starting from low energies, can be shown in the conventional way, as given in Fig. 3, *b*. More insight into the phenomena taking place is derived if the same infromation is plotted in a pseudo 3*D* plot exhibited above that, Fig. 3, *a*. While abscissa and ordinate mark the probe- and pump-light energies, respectively, the grey shading indicates the absorption changes, their calibration given by the bar at the top. In the experiment, the pump energy is raised successively by the steps marked with the short horizontal thin lines along the ordinate. The indicated diagonal, defined by identical probe- and pump-light energies $E_{\text{probe}} = E_{\text{pump}}$, is an important guideline allowing to organize the features in the plot. The absorption minima or, alternatively, the light-induced transparencies lying on the diagonal have to be attributed to primary processes. Here, a given pump energy photoionises a defect and the corresponding absorption, caused by this charge transfer, decreases. Such primary processes are marked by double arrows in Fig. 1. Secondary processes are those triggered by the primary ones; they are lying outside the diagonal in Fig. 3, *a*; among them are those given by single arrows in Fig. 1.

Along the vertical line in Fig. 3, *a*, crossing the minimum at $E_{\text{probe}} = E_{\text{pump}} = 1.9$ eV, the correlation with the EPR spectra of Rh^{4+} [12] was studied. The intensities of the corresponding EPR and absorption signals are given in Fig. 4. A close correlation is seen, supporting the assignment to Rh^{4+} being converted to Rh^{3+} by photoexcitation of a valence band electron, see lower part of Fig. 4. There also the corresponding process in real space is shown. In this and comparable investigations it should be kept in mind that the most intense absorption processes, such as charge transfer transitions, dominate the weaker ones, such as crystal field excitations. The latter can thus be neglected.

The conversion of Rh^{4+} creates Rh^{3+} and a hole in the valence band. Since an optical absorption band near 3.0 eV rises in parallel to the decrease of the Rh^{4+} absorption near 1.9 eV, it is likely that the band near 3.0 eV has to be attributed to Rh^{3+}. The hole in the valence band is not stable. Rather, it will be captured at a suitable trap. As Rh is the main impurity in the material, it is likely that the hole is caught at another Rh^{4+}, forming Rh^{5+}. The corresponding band, also rising essentially parallel to the decrease of Rh^{4+}, is seen to lie near 1.7 eV. This assignment of the Rh absorption bands is also supported by the fact that the higher valence, Rh^{5+}, has a lower absorption energy that Rh^{3+}. It takes less energy to excite a valence electron to a highly charged cation defect than to a lower charged one. The described primary charge transfer process and its secondary consequences comply with the 3-valence model, Fig. 1. One should note that also the EPR silent charge states Rh^{3+} and Rh^{5+} have become accessible

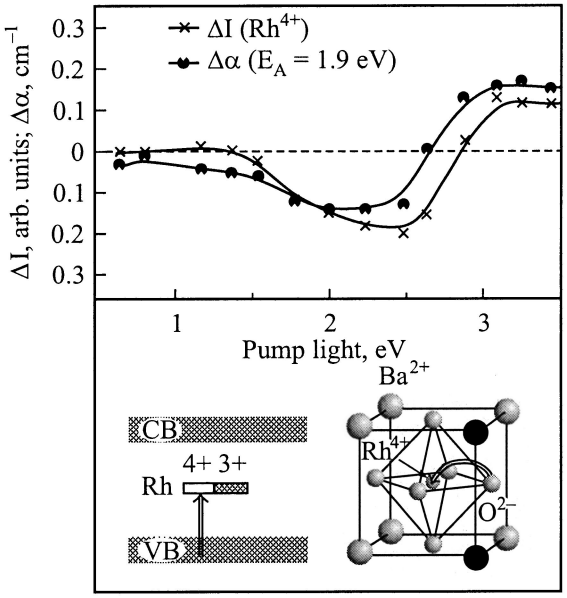

Figure 4. Comparison of light-induced changes of the Rh^{4+} EPR-signal and the optical absorption along the vertical line in Fig. 3. A close correlation between both signals is seen. The optical absorption band at 1.9 eV can thus be attributed to the indicated transfer of valence electrons to Rh^{4+}, shown in two equivalent ways in the lower panel.

by their optical fingerprints by this consistent interpretation procedure.

From Fig. 3 it is furthermore seen that not all absorption changes can be attributed to Rh charge states. The presence of unintended Fe background impurities must also be considered. This if based on previous work on this element in $BaTiO_3$ [4]. There, it was shown that Fe^{4+} is converted to Fe^{3+} near 2.6 eV. Fe^{5+} is recharged to Fe^{4+} near 2.3 eV. The charge transfer absorption of Fe^{3+} to Fe^{2+} is peaked at energies higher than 3.5 eV [13], lying above the band edge of $BaTiO_3$, about 3.2 eV, and thus lies outside of the graph in Fig. 3. The assignment of the features in Fig. 3 includes the Fe^{4+} and Fe^{5+} absorptions. It should be noted that Fig. 3 contains difference shectra; therefore the extrema in this plot can occur at energies slightly different from those of the component bands.

If the pump energy is changed, other charge transfer transitions will be activated as primary processes. Accordingly, the difference spectra will be composed of varying combinations of the component bands. The graphs at the right side of Fig. 3 illustrate this. As an example the consequences of the illumination at 2.4 eV are discussed: Here a primary process involving the low-energy outskirts of the Fe^{4+} absorption, subtracted from the Rh^{3+} band near 3.0 eV, is dominant. Pumping with 2.4 eV thus reduces the concentration of Fe^{4+}, present in the crystal from the beginning or created from Fe^{3+} by hole capture during the previous illumination with lower pump energies; the valence band holes are captured by Rh^{3+}, forming Rh^{4+}.

Also a diagram is given, qualitatively explaining the charge transfer processes triggered by 2.9 eV pump light. Here the fundamental absorptions starts, creating holes which are eventually increasing the concentrations of the higher valences of Rh and Fe. In assessing the right side of Fig. 3 is must be considered that — because of the Franck–Condon principle — optical and thermal levels have to be distinguished: primary transfers excite valence electrons to optical levels, whereas recombination to the valence band starts from thermal levels.

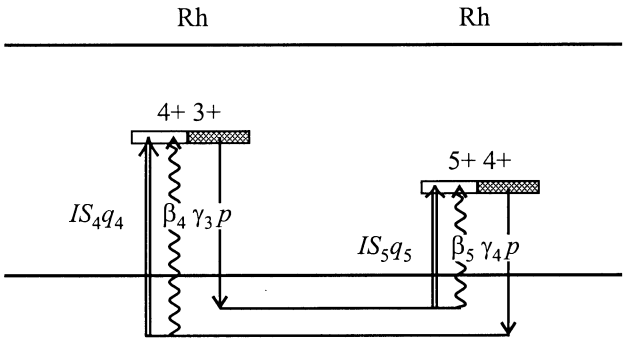

$$\dot{Rh}^{3+} = (IS_4q_4 + \beta_4)\ Rh^{4+} - \gamma_3 p\ Rh^{3+}$$
$$\dot{Rh}^{5+} = -(IS_5q_5 + \beta_5)\ Rh^{5+} + \gamma_4 p\ Rh^{4+}$$
$$\dot{Rh}^{4+} = -\ \dot{Rh}^{3+} - \dot{Rh}^{5+}$$

Figure 5. 3-valence model together with the set of differential equations governing the recharging of the Rh levels following thermally (wavy arrows) and optically (double arrows) induced transfer processes. For simplicity optical and thermal levels have not been distinguished.

3. Quantitative analysis

Assuming that all absorption bands represented by the features in Fig. 5 are caused by the five components Rh^{5+}, Rh^{4+}, Rh^{3+}, Fe^{5+} and Fe^{4+}, and for simplicity assuming gaussian band shapes, the plot (Fig. 3) can be analysed into the Rh^{i+} bands shown in Figs. 3, *c* and 6. Since the optical absorption of a defect '*i*' is connected to its density N_i by $\alpha_i(E) = N_i \cdot S_i(E)$, the energy dependence of the absorption cross-sections, $S_i(E)$, is given by that of the component absorption bands in Fig. 6. It the respective defect concentrations N_i are known, the cross-sections can be derived quantitatively.

In order to establish this quantitative calibration, the EPR signal of Rh^{4+}, for experimental reasons being given by the first derivative of the resonant microwave absorption, is integrated twice. This number, proportional to the amount of spins in the sample, is compared to the corresponding quantity of a known number of spins of a paramagnetic EPR standard. For this purpose small single crystals of $CuSO_4 \cdot 5H_2O$ of defined weight were used. On this basis the Rh^{4+} density in the material is determined [14].

Then, the change of the Rh^{4+} EPR signal under illumination with 1.9 eV light is compared to the correlated change of the Rh^{4+} optical absorption hand. Since the decrease of the number of Rh^{4+} ions can be inferred from the provious EPR calibration, the procedure allows to derive values of the absorption cross-section of Rh^{4+}, as given in Fig. 6. Their energy dependence is given by the gaussian fit. Assuming as an approximation, that the participation of the Fe charge states in Fig. 3 is only a minor effect, the validity of the 3-valence model can be taken as the basis for the further arguments. Since in this model two Rh^{4+} ions are converted to Rh^{3+} and Rh^{5+}, respectively, the changes of the concentrations under illumination with 1.9 eV, inducing the Rh^{4+} primary charge transfer process, are:
$\Delta Rh^{5+} = \Delta Rh^{3+} = -1/2\,\Delta Rh^{4+}$. By comparing the concentration changes to those of the corresponding absorption bands in Fig. 3, the absorption cross-section of Rh^{3+} and Rh^{5+} are derived. They are also given in Fig. 6.

With these quantities available, the concentrations of Rh^{3+}, Rh^{4+} and Rh^{5+} present in the crystal before illumination can now be determined. From the total absorption of the crystal one finds the values included

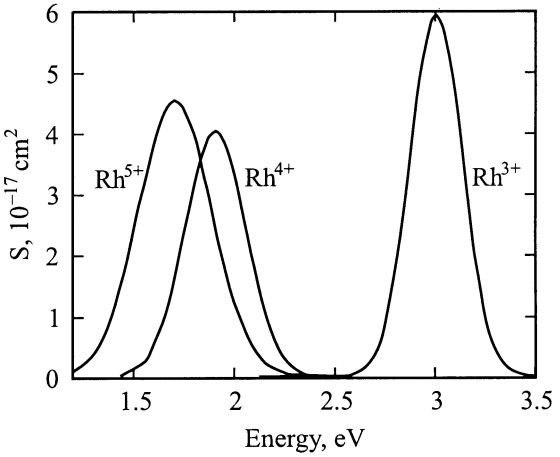

Figure 6. Energy dependence of the optical absorption cross-sections of the three Rh charge states involved.

in the Table. One deduces a total Rh concentration, $Rh_T = Rh^{3+} + Rh^{4+} + Rh^{5+}$, of about 40 ppm.

All the parameters governing the charge transfer processes connected with the 3-valence model, as applicable in first approximation ot BT:Rh, are comprised by the corresponding system of differential equations [2] displayed in Fig. 5. These rate equations describe the kinetics of the Rh charge states; the symbols have the following meanings ('*i*' indicating the Rh charge state species): Rh^{i+} — density of the charge state; I — light intensity; S_i — absorption cross-sections; q_i — probabilities that charge state '*i*' is ionised after absorption; β_i — thermal

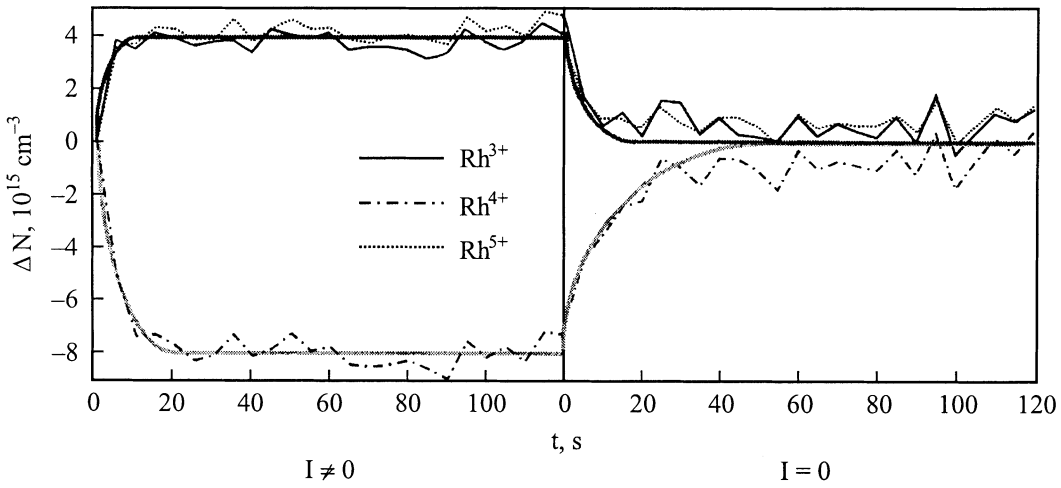

Figure 7. Rise ($I \neq 0$) and decay ($I = 0$) of the light-induced changes of the Rh^{5+}, Rh^{4+} and Rh^{3+} concentrations. The metastable deviation of the steady state changes under $I = 0$ from the equilibrium, expected to be zero, is small (about 1%) compared to the unchanged background of Rh^{i+}. Therefore, this small deviation is neglected.

ionisation rates; γ_i — capture coefficients; p — hole density in valence band.

Fig. 7 displays the corresponding changes of the defect densities, induced by illumination with 12 mW/cm^2 HeNe light and their decay after ending the illumination. It surprises that at room temperature they do not return to the initial state in the latter situation. Apparently this represents a metastable non-equilibrium situation, caused by a slow back reaction in the dark. The mobility of holes, thermally excited to the edge of the valence band, is more impeded by potential fluctuations than the mobility of holes light-induced during the forward reaction. This argument is supported by the data taken at 50°C. Here the changes relax to essentially zero because the hole mobility is increased at elevated temperatures even in the presence of potential fluctuations. Because then also the recombination processes are faster, the steady state amplitudes of the changes are smaller than at room temperature.

However, it should be considered that the light-induced absorption changes shown in Fig. 7 amount not only about 1% of the initial Rh^{i+} concentrations. Neglecting this very small relative mismatch between zero and the steady state values, the parameters listed in the Table were identified by fitting the numerical solutions of the rate equations to the data. The analysis of the photorefractive properties of the investigated specimen is in progress. Comparison with present results will take place when the necessary data is available.

Parameters describing charge transfer processes in $BaTiO_3$ involving Rh charge states

Generally valid parameters		Parameters characteristic for the investigated crystal (initial Rh concentrations)	
q_4	0.5	Rh^{4+}	$1.0 \cdot 10^{17}$ cm^{-3}
q_5	0.5	Rh^{3+}	$4.0 \cdot 10^{17}$ cm^{-3}
β_4	$9.3 \cdot 10^{-2}$ s^{-1}	Rh^{5+}	$0.5 \cdot 10^{17}$ cm^{-3}
β_5	1.3 s^{-1}	Rh_T	$5.5 \cdot 10^{17}$ cm^{-3} (= 40 ppm)
γ_3	$1.4 \cdot 10^{-12}$ cm^3/s		
γ_4	$3.9 \cdot 10^{-11}$ cm^3/s		
$S_i(E)$	see Fig. 6.		

4. Discussion

The basis of the presented method is the use of optical absorption bands as fingerprints of the existing defects, established byt means of the available EPR information. As shown, also EPR-silent lattice irregularities can often be labelled and identified on this way. In this manner the scope of defect studies is extended beyond that accessible to EPR measurements. The range of detectable defects is more than doubled because now it is possible also to verify the presence of the EPR-silent majority of defects. The method is applicable if the light-induced defect recharging leads to a photochromic situation. This is not a serious limitation, however. If not fulfilled at room temperature, this condition is usually valid at low temperatures where shallow traps tend to be populated by charge carriers after photoexcitation, while being empty at room temperature. From defect investigations under such conditions one can then extrapolate to the behaviour at room temperature where photorefractive devices are expected to operate.

There have been previous studies of $BaTiO_3$: Rh in which the charge transfer parameters responsible for the photorefractive properties of the material have been derived [9,10]. The present investigation differs from these studies in two respects. 1) Previously data from photorefractive measurements were used to derive — in a rether indirect way — the denstities of the defect charge states involved. Our present treatment obtains these densities independently and

can thus eventually check whether the photorefractive data are reproduced. 2) Based on the energy dependence of the defect-related optical cross-sections we get the quantitative information on the parameters of the light-induced charge transfer processes for a wide range of light energies. In each of the previous studies the analysis was limited to one light energy only.

Concluding, we have described a method by which the charge transfer processes occurring in doped insulating crystals can be analysed with respect to paths photoexcited charge carriers are taking between the involved defects. The method allows the quantitative determination of the parameters governing such processes. It is entirely based on the EPR information on the defects. Eventually it can lead to a prediction of the sensitivity of a doped photorefractive material.

References

[1] Photorefractive Effects and Materials / Ed. by P. Günter, J.-P. Huignard. Topics in Applied Physics 61, Springer (1988).
[2] K. Buse. Appl. Phys. **B64**, 273; 391 (1997).
[3] O.F. Schirmer, H.-J. Reyher, M. Wöhlecke. In: Insulating Materials for Optoelectronics / Ed. by F. Agulló-López. World Scientific (1995).
[4] O.F. Schirmer, M. Meyer, A. Rüdiger, C. Veber, A. Mazur. Optical Materials, in print.
[5] O.F. Schirmer. In: Defects and Surface-Induced Effects in Acvanced Perovskites. Kluwer (2000). P. 75.
[6] G.W. Ross, P. Hribek, R.W. Eason, M.H. Garrett, D. Rytz. Opt. Commun. **11**, 60 (1993).
[7] B.A. Wechsler, M.B. Klein, C.C. Nelson, R.N. Schwartz. Opt. Letters 536 (1994).
[8] M. Kaczmarek, R.W. Eason. Opt. Letters. 1850 (1995).
[9] N. Huot, J.M.C. Jonathan, G. Roosen. Appl. Phys. **B65**, 489 (1997).
[10] L. Corner, R. Ramos-Garcia, A. Petris, M.J. Damzen. Opt. Commun. **143**, 168 (1997).
[11] H. Kröse, R. Scharfschwerdt, A. Mazur, O.F. Schirmer. Appl. Phys. **B67**, 79 (1998).
[12] E. Possenriede, P. Jacobs, H. Kröse, O.F. Schirmer. J. Phys.: Condens. Matter **4**, 4719 (1992).
[13] H.J. Reyher, N. Hausfeld, M. Pape. J. Phys.: Condens. Matter **12**, 10 599 (2000).
[14] J.A. Weil, J.R. Bolon, J.E. Wertz. Electron Paramagnetic Resonance, Wiley (1994). P. 498.